# Quantum Trajectory in Multi-Dimensional Non-Linear System

Hiroto Kubotani \*
Faculty of Engineering, Kanagawa University, Yokohama 221-8686, Japan
(November 13, 2018)

We discuss quantum dynamics in multi-dimensional non-linear systems. It is well-known that wave functions are localized in a kicked rotor model. However, coupling with other degrees of freedom breaks the localization. In order to clarify the difference, we describe the quantum dynamics by deterministic rigid trajectories, which are accompanied with the de Broglie-Bohm interpretation of quantum mechanics, instead of wave functions. A bundle of quantum trajectories are repulsive through quantum potential and flow never to go across each other. We show that, according to the degrees of freedom, this same property appears differently.

03.65.B2, 05.45.MT, 05.45.-a

### I. INTRODUCTION

When the question "What is quantum chaos?" is thrown to us, we usually answer that no chaos is found in the quantum world. Successively, we cite a kicked rotor model [1] as a typical example. Its classical dynamics is reduced to the standard map, which is a well-known chaotic system. For a classical ensemble of the initial state, the dispersion of the momenta eternally continues to increase as a result of a random walk. For a quantized kicked rotor, however, numerical simulation reveals that the diffusion in the momentum space begins to be saturated after a time scale, and the wave function is found to be finally localized [2] [3]. Non-existence of quantum chaos can be also explained in general terms. For an isolated bound system, the energy spectrum is discrete and almost periodicity appears in the evolution of the wave function even if the energy spectrum is coarse-grained [4]. Further, even if the potential is allowed to be temporally periodic, the wave function of the bound states also evolves almost periodically as long as the system is not resonant [5]. In the proofs of these theorems, the property that the Schrödinger equation is a kind of wave equation and a wave function is a superposition of the oscillating solutions works as fundamental one to quantum mechanics. Therefore, quantum chaos is occasionally called quantum chaology or quantum psuedochaos [3] [6]. As reflection of this situation, the energy level statistics and the complex structure of eigenfunctions in quantum non-linear systems [3] rather than the dynamics have been searched for remnants of classical chaos.

A decade ago, Adachi, Toda, and Ikeda [7] [8] analyzed a system of coupled kick rotors which are classically chaotic. They found that localization of wave functions is broken in the model, while it appears when the coupling between the two rotors is absent. Then, Ikeda, Adachi, and Toda [9] showed that a quantum system with helper degrees of freedom monotonously absorbs energy from the external field [10]. Recently, Kubotani, Okamura, and Sakagami [11] have proposed that the coupled kicked rotors also yield quantum noise with decaying correlation and break irreversibly the quantum coherence in contacted other degrees of freedom. These results show that redundant degrees of freedom may drastically alter the quantum dynamics. Further, if we are allowed to apply the Schrödinger equation to the whole universe, which is isolated and composed of infinitely many degrees of freedom, the fundamental questions arises: Why some degrees of freedom behave classically and others quantum-mechanically? Why only the formers are able to behave chaotically or irreversibly? These problems cannot be answered straightforwardly [12]. Even without taking the ideal and mathematical limit of infinite degrees of freedom a priori, therefore, the quantum dynamics still involves important and interesting phenomena, although chaos in the exact sense, which is believed to contribute to irreversibility in the classical world [13], may not be present in the quantum world.

According to the de Broglie-Bohm interpretation of quantum mechanics [14], we can introduce a bundle of rigid trajectories which are consistently equivalent to a wave function. At first sight, the rigidity may be inconsistent with the uncertainty principle in quantum mechanics. Indeed, the uncertainty principle makes a product of the expected values of canonically conjugated variables superior to the Planck constant  $\hbar$ . In the Copenhagen interpretation, the relation is considered as inaccuracy of the simultaneous measurement of the conjugate variables. However, there is no mathematical inconsistency between the quantum trajectory picture and the time evolution of a wave function driven by the Schrödinger equation as will be seen in Section 2. The de Broglie-Bohm interpretation considers quantum

<sup>\*</sup>e-mail address: kubotani@yukawa.kyoto-u.ac.jp

expectation values as statistically averaged ones and thus the apparent inconsistency is due to the confusion of the measurement theories on which we base the interpretation of the uncertainty relation.

Although the recovery of classical diffusion is confirmed by the previous works [7]- [12], it does not necessarily mean that the classical dynamics is restored in quantum mechanics. The dynamics needs to be estimated more directly. The associated problems to be resolved are how nonlinearity work in quantum systems and what role redundant degrees of freedom play. In order to reveal them, in this paper, we propose to utilize quantum trajectories. For analysis of wave functions, indeed, the Wigner and Husimi functions have been used [16]. These projective representations of wave functions on the phase space can be compared with classical statistical distributions. However, since they do not follow the Liouville equation, the comparison estimates only the correspondence or difference in the snap shot between the classical and quantum states. For the analysis of the dynamics, therefore, the description of quantum mechanics by trajectories is favorable, since the trajectories can be easily compared with classical orbits. By the quantum trajectory picture, even the standard notions of chaos, such as the Lyapnov index and the KS entropy are also introduced naturally into the quantum world [15].

This paper is organized as follows. In the section 2, we introduce a coupled kicked rotator model as a multidimensional non-linear system and discuss the quantum picture of trajectories. We calculate the quantum trajectory of the system in the section 3. In the section 4, we give the summary and discuss the results.

## II. MULTI-DIMENSIONAL NON-LINEAR MODEL

The kicked rotor model was first introduced by Chirikov [1]. Its property has been widely investigated both in classical and quantum mechanics, since it has the dynamics which is typical of nonlinear systems. The Hamiltonian is

$$H_k(q, p; t) = \frac{1}{2}p^2 + k\cos(q)\sum_{n=1}^{\infty} \delta(t - nT) \quad (0 \le q < 2\pi),$$
(2.1)

where q and p are an angle variable with period  $2\pi$  and its canonically conjugated action variable, respectively, and k and T are constant. The first term is quadratic with respect to the action variable p and shows a nonharmonic oscillator. Alternatively we can also consider it as the kinetic term with respect to the momentum p. The second one shows the temporally periodic and instantaneous kick, whose strength and period are parameterized by k and T, respectively. The classical dynamics is reduced to a discretized map. The variables  $(q_n, p_n) \equiv (q(t = nT + 0), p(t = nT + 0))$  at the discretized time t = nT + 0  $(n = 0, 1, 2, \cdots)$  are transformed as

$$q_{n+1} = q_n + Tp_n,$$
  
 $p_{n+1} = p_n + k\sin(q_{n+1}).$  (2.2)

Here +0 indicates the time just after the kick. The transformation rule (2.2) is called the standard map, whose dynamics is characterized by one parameter  $K \equiv kT$ . When  $K \lesssim 1$ , the variables  $(q_n, p_n)$  are trapped on the KAM torus. When K exceeds the critical value  $K_{cr} = 0.9716 \cdots$ , they diffuse into the chaotic sea on the phase space.

We couple two kicked rotors whose kick strengths are  $k_1$  and  $k_2$ . The total Hamiltonian of the coupled rotors is given by

$$H(q_1, p_1, q_2, p_2; t) = H_{k_1}(q_1, p_1; t) + H_{k_2}(q_2, p_2; t) + H_{int}(q_1, p_1, q_2, p_2; t).$$
(2.3)

This type of model has been used by Adachi et al [7], Kubotani et al [11], and Sakagami et al [12]. In this paper we choose the interaction Hamiltonian  $H_{int}$  as

$$H_{int}(q_1, p_1, q_2, p_2; t) = c_{pp} p_1 p_2, (2.4)$$

where  $c_{pp}$  is a coupling constant. The interaction Hamiltonian  $H_{int}$ , Eq. (2.4) causes continuous interaction between the two degrees of freedom through the action variables  $p_1$  and  $p_2$ . Hereafter we call the coupled kick rotors as a pp-coupling model.

We quantize the coupled kicked rotors (2.3). In the Shrödinger picture, we write down the time evolution operator as

$$\hat{U}(t) = T_{O} \exp\left[-\frac{i}{\hbar} \int_{0}^{t} ds \hat{H}(s)\right], \tag{2.5}$$

where  $T_O$  denotes the time ordered product, and  $\hat{H}(t)$  is the quantized Hamiltonian operator which is derived by replacing the canonical variables  $q_1$ ,  $q_2$ ,  $p_1$ , and  $p_2$  in Eq.(2.3) with the corresponding quantum operators  $\hat{q_1}$ ,  $\hat{q_2}$ ,  $\hat{p_1}$ , and  $\hat{p_2}$ . In general, incommutability between the conjugate operators in the Hamiltonian complicates estimation of the time ordered product. For the pp-coupling model, we only have to take account of the ordering at the time when the kick is added. As a result, the operator (2.5) is reduced to a simple form

$$\hat{U}(t) = \hat{U}_1(t_0)(\hat{U}_2\hat{U}_1(T))^n, \tag{2.6}$$

where

$$\hat{U}_1(t) \equiv \exp\left[-\frac{i}{2\hbar}(\hat{p}_1^2 + \hat{p}_2^2 + 2c_{pp}\hat{p}_1\hat{p}_2)t\right],\tag{2.7}$$

$$\hat{U}_2 \equiv \exp[-\frac{i}{\hbar}(k_1\cos(\hat{q}_1) + k_2\cos(\hat{q}_2))].$$
 (2.8)

Here  $t_0 \equiv t - n_0 T$  and  $n_0 = [t/T]$ , where [x] denotes the maximum integer which is not superior to x. Note that the operators  $\hat{U}_1$  and  $\hat{U}_2$  are constructed only from the the action variable operators  $\hat{p}_1$  and  $\hat{p}_2$  or the angle variable operators  $\hat{q}_1$  and  $\hat{q}_2$ , respectively, and can be expressed as diagonal matrices by choosing an appropriate representation. Therefore, the operation of Eq. (2.6) to a wave function is decomposed into the two procedures: the interchange of the representation of the wave function and the multiplication of complex factors. The simplicity guarantees low roundoff error in the numerical simulation of a wave function.

According to the de Broglie-Bohm interpretation of quantum theory [14], we construct a bundle of deterministic rigid trajectories from a wave function in the pp-coupling model. First, we express the wave function with respect to the polar coordinate:

$$\Phi(q_1, q_2; t) = R(q_1, q_2; t) \exp\left[\frac{i}{\hbar} S(q_1, q_2; t)\right], \tag{2.9}$$

where the  $q_1, q_2$  representation is chosen, and R and S are real-valued functions. Using this expression, we decompose the Schrödinger equation into two parts:

$$\frac{\partial}{\partial t}R^2 + \frac{\partial}{\partial q_1}R^2((\frac{\partial S}{\partial q_1}) + c_{pp}(\frac{\partial S}{\partial q_2})) + \frac{\partial}{\partial q_2}R^2((\frac{\partial S}{\partial q_2}) + c_{pp}(\frac{\partial S}{\partial q_1})) = 0, \tag{2.10}$$

and

$$\frac{\partial S}{\partial t} + \frac{1}{2} \left(\frac{\partial S}{\partial q_1}\right)^2 + \frac{1}{2} \left(\frac{\partial S}{\partial q_2}\right)^2 + c_{pp} \left(\frac{\partial S}{\partial q_1}\right) \left(\frac{\partial S}{\partial q_2}\right) + V(q_1, q_2; t) + V_Q(q_1, q_2; t) = 0, \tag{2.11}$$

where  $V(q_1, q_2; t)$  is a original potential:

$$V(q_1, q_2; t) = (k_1 \cos(q_1) + k_2 \cos(q_2)) \sum_{n=1}^{\infty} \delta(t - nT),$$
(2.12)

and  $V_Q(q_1, q_2)$  is what we call a quantum potential:

$$V_Q(q_1, q_2; t) = -\frac{1}{2R} \left( \frac{\partial^2 R}{\partial^2 q_1} + \frac{\partial^2 R}{\partial^2 q_2} + 2c_{pp} \frac{\partial^2 R}{\partial q_1 \partial q_2} \right) \hbar^2. \tag{2.13}$$

Next, we consider an ensemble consisting of quantum particles with the initial distribution function  $R(q_1, q_2; t = 0)^2$ . For the particles, we can define rigid trajectories as follows. The momentum  $(p_1, p_2)$  of a particle on a trajectory is equalized to the spatial gradient of the phase part of the wave function, S:

$$p_i = \left(\frac{\partial S}{\partial q_i}\right) \quad (i = 1, 2). \tag{2.14}$$

From the Hamilton's canonical equation, the particle moves according to the velocity:

$$\dot{q}_1 = p_1 + c_{pp}p_2 = \left(\frac{\partial S}{\partial q_1}\right) + c_{pp}\left(\frac{\partial S}{\partial q_2}\right),$$

$$\dot{q}_2 = p_2 + c_{pp}p_1 = \left(\frac{\partial S}{\partial q_2}\right) + c_{pp}\left(\frac{\partial S}{\partial q_1}\right).$$
(2.15)

Integration of Eq. (2.15) with respect to t yields a time-parameterized trajectory. The relation (2.15) allows Eq. (2.10) to be rewritten as

$$\frac{\partial}{\partial t}R^2 + \frac{\partial}{\partial q_1}\dot{q}_1R^2 + \frac{\partial}{\partial q_2}\dot{q}_2R^2 = 0, \tag{2.16}$$

which reserves conservation of the distribution function  $R(q_1, q_2; t)^2$ . We also note that Eq. (2.11) corresponds to the Hamilton-Jacobi equation in classical mechanics. Compared with the classical one, the additional term  $V_Q$  appears in Eq. (2.11). The term shows quantum effect on quantum trajectories. That is why  $V_Q$  is called a quantum potential. We mention that Eq. (2.14) appears to show WKB approximation. By definition, however, S is not equivalent to the phase part of the WKB wave function,  $S_{WKB}$ .  $S_{WKB}$  is determined by the classical Hamilton-Jacobi equation which does not include the quantum potential  $V_Q$ . Therefore, only if  $V_Q$  is negligible, S happens to be equal to  $S_{WKB}$ . In other words, the quantum trajectory picture is not limited to WKB regions and always defined consistently irrespective of any approximation schemes.

### III. QUANTUM TRAJECTORY IN NON-LINEAR SYSTEM

In this section, we numerically trace quantum trajectories in the coupled kick rotor model constructed in the section 2 and compare them with classical ones. For this aim, we first solve the original Schrödinger equation instead of the quantum Hamilton-Jacobi equation (2.11). To represent a wave function numerically, we use  $4096 \times 512$  mesh points. Setting  $\hbar = 2\pi \times 43/4096 = 0.0659 \cdots$ , we can describe the momentum eigenstates with the eigenvalues  $p_1$  from  $-43\pi$  to  $43\pi$  and  $p_2$  from  $-43\pi/8$  to  $43\pi/8$ . For the model to analyze, we fix the parameters as  $k_1 = 2.0$ ,  $k_2 = 0.9$ , and T = 1.0. As an initial wave function, we choose a product of the momentum eigenstates for each degree of freedom:

$$\Phi_0(q_1, q_2) = \Phi_{p_{1_0}}(q_1) \otimes \Phi_{p_{2_0}}(q_2) 
= \frac{1}{\sqrt{2\pi}} \exp(-\frac{i}{\hbar} p_{1_0}(q_1 - \frac{\pi}{4})) \times \frac{1}{\sqrt{2\pi}} \exp(-\frac{i}{\hbar} p_{2_0}(q_2 - \frac{\pi}{4})),$$
(3.1)

where  $p_{10}$  and  $p_{20}$  are initial eigenvalues. In the following concrete calculation, we set  $p_{10} = p_{20} = \pi/2$ . The wave function at the arbitrary time is obtained by multiplying the initial wave function by the operator (2.6). From the time-dependent wave function, next, we estimate the velocity of a quantum particle, (2.15). The spatial derivative of the wave function just on the mesh point is estimated by the inverse Fourier transformation. The value between the mesh points is interpolated [17]. A quantum trajectory is calculated by integrating the velocity field by the Rungge-Kutta method.

We begin by observing gross time evolution of quantum state with respect to the dispersion of the momentum  $\hat{p}_1$ . Fig. 1 shows the second order moment  $Q \equiv <(\hat{p}_1-<\hat{p}_1>)^2>$ , where <> denotes the expectation value estimated with respect to the wave function at the time t=nT+0. The lines (No) and (P-P) indicate the single kick rotor model  $(k_1=2.0,\,c_{pp}=0)$  and the pp-coupling model  $(k_1=2.0,\,k_2=0.9,\,$  and  $c_{pp}=0.2)$ , respectively. For the single rotor, localization of a wave function is found. For the coupled kicked rotors, on the other hand, the diffusion in the momentum space seems to continue. In Fig. 2, the distribution of the momentum  $\hat{p}_1$  at t=100T+0,  $|< p_1|\Phi(t=100T+0)>|^2$  is shown for each model. The distribution (No) is approximate to  $\ln|< p_1|\Phi>|^2 \propto -|p_1|$ , although the classical law for the chaotic rotor would be  $\ln f(p) \propto -p^2$ , where f(p) is a classical distribution function. Comparison with the quantum kicked rotor modulated by classical noise is discussed in [8].

Fig. 1 shows that introduction of coupling with other degrees of freedom may change the quantum dynamics drastically. However, the recovery of classical diffusion found here does not necessarily mean that the Liouville dynamics is restored in the evolution of the wave function. Fig. 2 shows the plateau with  $2\pi$  period appears in the distribution for the coupled rotors. As well as Fig. 1, it suggests similarity between the classical and quantum dynamics [8].

The classical dynamics of a single kicked rotor is reduced to a map between the variables at discretized time as mentioned in the section 2. For the coupled kicked rotors (2.3), the map is

$$q_{i,n+1} = q_{i,n} + Tp_{i,n} + c_{pp}p_{j,n} (i = 1, 2, j \neq i),$$
  

$$p_{i,n+1} = p_{i,n} + k_i \sin(q_{i,n+1}), (3.2)$$

where  $(q_{i,n}, p_{i,n}) = (q_i(t = nT + 0), p_i(t = nT + 0))$  are the canonical variables at the discretized time t = nT + 0 (n=0, 1, 2, ···). The classical particle in the region  $[0, \pi]$  is accelerated and one in the region  $[\pi, 2\pi]$  is decelerated by

a kick. Until the next kick, the momentum is conserved and the velocity of the particle is constant. The dynamics results in effective stretching and folding of a phase space volume element.

For the quantum particle, on the other hand, the velocity can be altered, even if the original potential in the Hamiltonian is not present. The instantaneous kick yields the inhomogeneous velocity field of the quantum particle. After the kick, as a result, the particles are gathered inhomogeneously and high density regions are produced. The gradient of the density of the particles gives nonzero quantum potential through Eq. (2.13). In other words, the quantum particle feels repulsive force from the other particles. Further, uniqueness of the solution of the differential equation (2.15) guarantees that two quantum trajectories cannot go across each other. Fig. 3 shows quantum trajectories just after the 1st kick. The lines in Fig. 3(a) are trajectories for the single rotor model with no coupling. At t = T, 20 particles are settled homogeneously between 0 and  $2\pi$  on the  $q_1$ -axis. Figs. 3(b) and 3(c) show typical quantum trajectories for the pp-coupling model. For Figs. 3(b) and 3(c), we set 20 particles evenly on the surfaces  $q_2 = \pi$  and  $q_2 = 0$ , respectively, at t = T. The strongly repulsive nature of the trajectory is observed in Fig. 3(a). Although the repulsion is also found in Fig. 3(b), for Fig. 3(c) it is partially milder than ones found in Figs. 3(a) and 3(b). For the coupled rotors, we also see the evolution of the quantum trajectory in the 2-dimensional configuration space  $(q_1, q_2)$  after the 1st kick. Fig. 4 shows the evolution of the 500 particles which are equally spaced on the surfaces  $q_2 = \pi$  and  $q_2 = 0$  at t = T as well as Figs. 3(b) and 3(c). The initial straight row of particles is going to be broken at the region where the particle density is increased by condensation of the quantum trajectories.

Next, we estimate effective acceleration of a quantum particle induced by a kick. In the classical system, nonlinearity in the kick is enhanced by the free motion after the kick. For a kicked rotor, therefore, the efficiency of the nonlinearity is parameterized by  $K \equiv kT$ , rather than bare kick strength k. In the quantum system, however, the free motion is suppressed by the quantum potential, as seen in Fig. 3. To quantify the effect, we propose to estimate the averaged velocity  $V_i(n)$  by the distance over which the quantum particle moves during the time interval [nT, (n+1)T]:

$$V_i(n) \equiv \frac{1}{T} (q_{i,n+1} - q_{i,n}). \tag{3.3}$$

Further, the change rate of the effective velocity  $V_i$  is considered as the effective strength of the impulsive kick. Therefore, we estimate the effective kick strength by

$$F_i(n) \equiv \frac{1}{T}(V_i(n) - V_i(n-1)) = \frac{1}{T^2}((q_{i,n+1} - q_{i,n}) - (q_{i,n} - q_{i,n-1})). \tag{3.4}$$

For the classical standard map (3.2),  $F_i$  is approximately a sine function with respect to  $q_{i,n}$ . For the quantum system, we calculate  $F_1(n)$  numerically. At the time  $t=30\mathrm{T}$ , when the difference in the dispersion  $<(\hat{p}_1-<\hat{p}_1>)^2>$  between the single rotor and the coupled ones is apparently observed (Fig.1), we let  $500\times20$  probe particles distributed uniformly on the  $q_1$ -coordinate for the single kick rotor, and on the configuration space  $(q_1,q_2)$  for the coupled kick rotor model. Figs. 5(a) and 5(b) are the results for the single kicked rotor and pp-coupling models, respectively. For some particles, the numerical estimation of  $V_1(29)$  and  $V_1(30)$  does not converge with respect to the integration step size, since they may go through the irregularly large quantum potential. In Fig. 5(b), we plot  $F_1(30)$  for the 9899 particles whose deviations in  $V_1(29)$  and  $V_1(30)$  are smaller than 0.1 if we make the integration step size half. For the coupled kick rotors, we can find the tendency that the particles in the region  $0 < q_1 < \pi$  are accelerated and ones in the region  $\pi < q_1 < 2\pi$  are decelerated, although not a few particles don't follow the tendency and the acceleration and deceleration amplitude is weaker than in the genuine classical case  $2.0 \sin(q_1)$ . The tendency is obscure in Fig.5(a) for a single rotor model.

We see the evolution of volume elements in the 2-dimensional configuration space  $(q_1, q_2)$ . At t = T, we distribute initial probe particles uniformly between 0 and  $2\pi$  on the surfaces  $q_2 = 2\pi \times \frac{i}{10}$  (i=0, 1, ..., 9) as shown in Fig. 6(a). Figs. 6(b) and 6(c) show snapshots on the configuration space  $(q_1, q_2)$  at t = 2T and t = 3T, respectively. The density of quantum particles is conserved in accordance with Eq. (2.10). The volume elements of the density in the configuration space obtain entanglement after several kicks.

In addition to the dynamics, we also check the distribution of the momentum of the quantum particle,

$$f_Q(p_1) = \int \int dq_1 dq_2 |\Phi(q_1, q_2)|^2 \delta(p_1 - \frac{\partial S}{\partial q_1}).$$
 (3.5)

By definition, it may differ from the amplitude of the wave function in the  $p_1$ -representation (Fig.2). The result is given in Fig.7.

#### IV. SUMMARY AND DISCUSSION

In order to recognize the role of nonlinearity in quantum systems, we estimated quantum trajectories for the coupled kick rotor model. It has recently been known phenomenologically that effect of the nonlinearity appears differently, depending on the degrees of freedom of a system [7]- [12]. In a single kicked rotor, for example, suppression of the momentum diffusion appears and the wave function is localized. For the coupled kick rotors, on the other hand, the diffusion in the momentum space seems to continue. In this paper, we compared the single rotor with the coupled rotor model from the viewpoint of quantum trajectories. For a single kick rotor, the acceleration of a quantum particle induced by the impulsive kicks is suppressed by the quantum potential(Fig. 3(a)). For the coupled two rotors, by contrast, entanglement in the two dimensional configuration space is realized (Fig. 6) and suppression of the acceleration by the kick is mild in spite of repulsion between trajectories(Fig. 3(c)). In fact, some particles are really accelerated (Fig. 5). The dispersion of the momentum of the particles is expanded by the kicks and localization is broken for the wave function (Fig. 1).

A bundle of quantum trajectories flow according to the continuity equation and each trajectory does never go across the others due to the uniqueness theory for solutions of differential equations [14]. In one dimensional system, this property appears as the phenomenon that the quantum trajectories are repulsive and the complicated density distribution tends to be flattened. Therefore, the relative acceleration between quantum particles induced by nonlinearity is suppressed in the system. This results in the localization of the wave function. For the system with redundant degrees of freedom like our coupled kick rotor model, the complicated density distribution is flattened also into the second degree of freedom. That is, quantum particles can be scattered forwardly with each other. As a result, the repulsive nature due to quantum interference is not straightforward. It is the reason why introduction of the coupling yields the possibility that some particles can be accelerated and the localization of the wave function is broken.

In the de Broglie-Bohm interpretation, the momentum of a quantum particle with a rigid trajectory is equalized to the spatial gradient of the phase factor in the wave function. In the pp-coupling model,

$$\ddot{q}_{2} = \dot{p}_{2} + c_{pp}\dot{p}_{1} = -\frac{\partial}{\partial q_{2}}V_{Q} - c_{pp}\frac{\partial}{\partial q_{1}}V_{Q}$$

$$= \frac{\hbar^{2}}{2}\frac{\partial}{\partial q_{2}}\frac{1}{R}\left(\frac{\partial^{2}R}{\partial q_{1}^{2}} + \frac{\partial^{2}R}{\partial q_{2}^{2}} + 2c_{pp}\frac{\partial^{2}R}{\partial q_{1}\partial q_{2}}\right) + \frac{\hbar^{2}c_{pp}}{2}\frac{\partial}{\partial q_{1}}\frac{1}{R}\left(\frac{\partial^{2}R}{\partial q_{1}^{2}} + \frac{\partial^{2}R}{\partial q_{2}^{2}}\right) + O(c_{pp}^{2}).$$

$$(4.1)$$

Equation (4.1) shows that, even if the degrees of freedom,  $q_1$  and  $q_2$  are uncorrelated initially, that is,  $R(q_1, q_2) = R(q_1)R(q_2)$ , the coupling induces the gradient of quantum potential with respect to the  $q_1$ -direction and accelerate particles in the direction of the second degree of freedom,  $q_2$ . This effect decreases the gradient of the density of quantum particles and reduces the repulsion in the  $q_1$ -direction. In the work by Adachi et al [7], the instantaneous coupling between the configuration variables  $q_1$  and  $q_2$  is introduced as a model to analyze. In this case, mixing of the phase factor in the wave function is induced directly by the coupling and causes the acceleration along the  $q_2$ -axis.

Redundant degrees of freedom help the classical diffusion, which is analogous to the ergodicity although the phase space is not compact in our model. Our analysis also shows that multi-dimensional systems emulate partly the classical dynamics. On one hand, the quantum trajectory is altered by repulsion in short range. In global range, on the other hand, it may express nonlinearity in the system. We may say that the Ehrenfest time scale is not active in our analysis where the wave function is spread widely from the beginning and continues diffusion in the uncompact phase space. Therefore, there is a possibility that we can treat the appearance of the classical property as a matter of the scale of the discrepancy between trajectories rather than a matter of the time scale, such as the Ehrenfest time scale. To clarify the dependence of the dynamics on the spatial discrepancy between quantum trajectories, we have to make further qualitative analysis. The analysis need more computational memory and more CPU time and will be presented elsewhere.

As demonstrated in this paper, the de Broglie-Bohm picture which gives rigid trajectories is helpful to understand the dynamics equivalent to the unitary evolution driven by the Schrödinger equation. In the quantum trajectory picture, however, the superposition of the right going and left going waves which have the same and opposite momentum is identified with the static state with zero momentum. In our analysis, therefore, we utilized the averaged velocity  $V_i$  rather than the velocity at a moment, (2.15). In Fig. 2, the characteristic plateaus appears at the classically forbidden point  $(q, p) = (\pi, 2n\pi)(n = 0, \pm 1, \pm 2, ...)$  which corresponds to the elliptical fixed point, while does not in Fig. 7. For comparison with the statistical distribution on the phase space, the Wigner and Husimi descriptions have certainly preferable points [18]. To understand the quantum dynamics in multi-dimensional non-linear systems further, the de Broglie-Bohm approach and complementally the Wigner and Husimi functions will be needed.

- [1] B. V. Chirikov, Phys. Rep. **52**, 263 (1979).
- [2] B. V. Chirikov, F. M. Izrailev, and D. L. Shepelyansky, Sov. Sci. Rev. Sect. C2, 209 (1981).
- [3] B. V. Chirikov, F. M. Izrailev, and D. L. Shepelyansky, Physica D33, 77 (1988).
- [4] I. C. Percival, J. Math. Phys. 2, 235 (1961).
- [5] T. Hogg and B. A. Huberman, Phys. Rev. Lett 48, 711 (1982).
- [6] G. Casatti and B. Chirikov, in Quantum chaos: between order and disorder (Cambridge Univ. Press, Cambridge, 1995).
- [7] S. Adachi, M. Toda, and K. Ikeda, Phys. Rev. Lett. 61, 655 (1988).
- [8] M. Toda, S. Adachi, and K. Ikeda, Prog. Theor. Phys. Supp. 98, 323 (1989).
- [9] K. Ikeda, S. Adachi, and M. Toda, Phys. Lett. A147, 189 (1990).
- [10] K. Ikeda, Phys. Lett. A168, 248(1992); K. Ikeda, Ann. Phys. 227, 1(1993).
- [11] H. Kubotani, T. Okamura, and M. Sakagami, Physica A214, 560 (1995).
- [12] M. Sakagami, H. Kubotani, and T. Okamura, Prog. Theor. Phys. 95, 703 (1996).
- [13] G. M. Zaslavsky, Chaos in dynamic systems (Nauka, Moscow, Russian, 1984).
- [14] P. R. Holland, The quantum theory of motion: an account of the de Broglie-Bohm causal interpretation of quantum mechanics (Cambridge Univ. Press, Cambridge, 1993).
- [15] U. Schwengelbeck and F. H. M. Faisal, Phys. Lett. A199, 281 (1995).
- [16] K. Takahashi and N. Saitô, Phys. Rev. Lett. 55, 645 (1985).
- [17] W. H. Press, S. A. Teukolsky, W.T. Vetterling, and B. P. Flannery, Numerical Recipes in Fortran(2nd) (Cambridge Univ. Press, Cambridge, 1992).
- [18] S. B. Lee and M. D. Feit, Phys. Rev. E 47, 4552 (1993); B. S. Helmkamp and D. A. Browne, Phys. Rev. E 49, 1831 (1994).
- FIG. 1. The time evolution of the dispersion of the momentum, the second order moment  $Q \equiv \langle (\hat{p}_1 \langle \hat{p}_1 \rangle)^2 \rangle$  is shown. The lines (No) and (P-P) indicate the quantum single kick rotor with the kick strength  $k_1 = 2.0$  and the kick rotors with the momentum coupling, respectively. For the coupled kicked rotors, the kick strength  $k_1$  and  $k_2$  are set to 2.0 and 0.9, respectively, and the coupling strength  $c_{pp}$  is 0.2. The initial state is set to the momentum eigenstate with  $p_{10} = p_{20} = \pi/2$  in Eq. (3.1).
- FIG. 2. The momentum distribution  $|\langle p_1|\Phi\rangle|^2$  at  $t=100\mathrm{T}+0$  are shown. The abbreviations (No) and (P-P) indicate the single kick rotor and pp-coupling models, respectively. The model parameters  $k_1$ ,  $k_2$ , and  $c_{pp}$  are the same as in Fig. 1.
- FIG. 3. The quantum trajectory during the time interval from t = T to t = 2T is shown. The horizontal axis indicates the time t, and the vertical one shows the  $q_1$ -coordinate. Fig. 3(a) shows the 20 typical trajectories which are set uniformly along the  $q_1$ -coordinate at t = T for a single rotor. By contrast, Figs. 3(b) and 3(c) show the 20 quantum trajectories which are equally spaced on the surfaces  $q_2 = \pi$  and  $q_2 = 0$ , respectively, at t = T. The model parameters  $k_1$ ,  $k_2$ , and  $c_{pp}$  are the same as in Fig. 1.
- FIG. 4. For the coupled kicked rotors, the time evolution of probe particles is shown in the time interval from t = T to t = 2T. At t = T, 1000 quantum particles are ranged homogeneously on the surfaces  $q_2 = \pi$  and  $q_2 = 0$ . The horizontal and vertical axes show the coordinates  $q_1$  and  $q_2$  of the probes, respectively. Each row like a line shows the snap shot at t = 1.0T, 1.1T, 1.2T, ..., 2.0T. The model parameters  $k_1$ ,  $k_2$ , and  $c_{pp}$  are the same as in Fig. 1.
- FIG. 5. The effective acceleration  $F_1(30)$  for  $500 \times 20$  probes which are settled at t = 30T is shown. Figs. 5(a) and 5(b) correspond to the single kick rotor and pp-coupling models, respectively. For the single kick rotor, the probes are distributed uniformly between 0 and  $2\pi$  along the  $q_1$ -axis. For the coupled kicked rotors, 20 rows which consists of 500 probes along the  $q_1$  axis are arranged uniformly between 0 and  $2\pi$ . For each probe, the averaged velocities  $V_1(29)$  and  $V_2(30)$  are estimated by the two computational runs which are different in the time step size ( $\Delta t = 2.5 \times 10^{-6}$ T and  $5.0 \times 10^{-6}$ T). For the coupled kicked rotor, the 101 probes whose deviations in  $V_1(29)$  and  $V_2(30)$  are greater than 0.1[1/T] are rejected in Fig. 5(b). The model parameters  $k_1$ ,  $k_2$ , and  $c_{pp}$  are the same as in Fig. 1.

- FIG. 6. The positions of  $5000 \times 10$  probes are shown to visualize the deformation of the volume element in the 2-dimensional configuration space  $(q_1, q_2)$ . Fig. 6(a) shows the initial positions of the probes distributed uniformly on the surface  $q_2 = 2\pi \times i/10 (i = 0, 1, \dots 9)$  at t = T. Fig. 6(b) and (c) are the snap shots for the positions of the probes at t = 2T and 3T, respectively. The model parameters  $k_1$ ,  $k_2$ , and  $c_{pp}$  are the same as in Fig. 1.
- FIG. 7. The distribution of the momentum of the quantum particles are shown. The distribution function is estimated by  $f_Q(p_1) = \int \int |\Phi|^2 \delta(p_1 \frac{\partial S}{\partial q_1}) \mathrm{d}q_1 \mathrm{d}q_2$ , where  $\Phi$  is the wave function at  $t = 100\mathrm{T}$  for the pp-coupling model. The model parameters  $k_1$ ,  $k_2$ , and  $c_{pp}$  are the same as in Fig. 1.

This figure "fig1.png" is available in "png" format from:

This figure "fig2.png" is available in "png" format from:

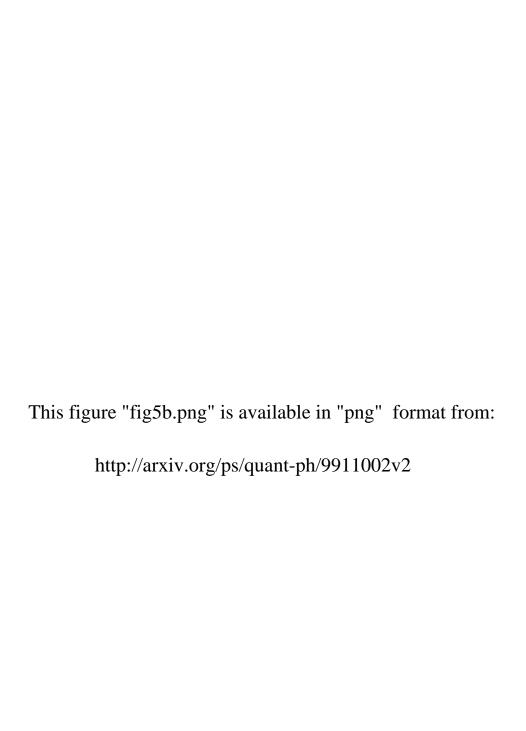
This figure "fig3a.png" is available in "png" format from:

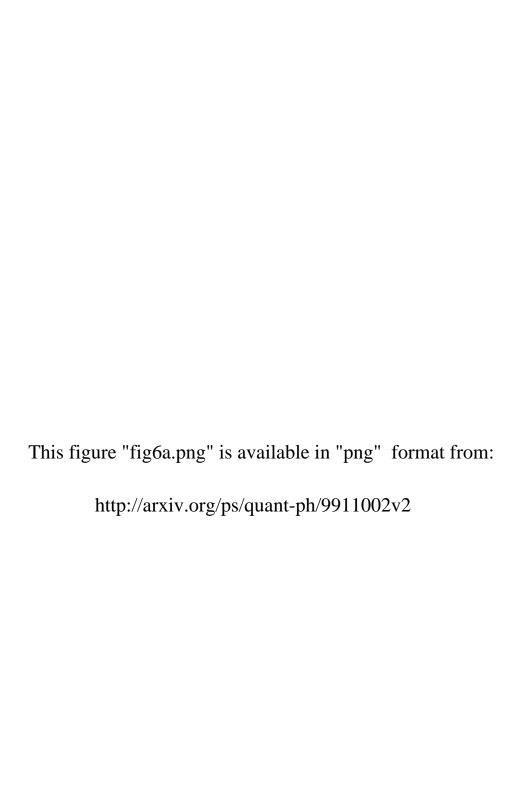
This figure "fig3b.png" is available in "png" format from:

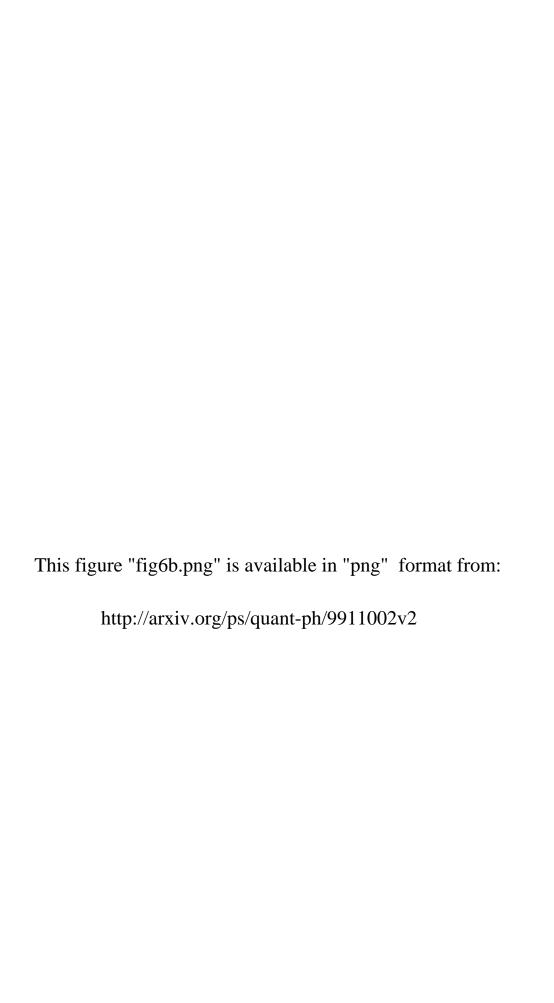
This figure "fig3c.png" is available in "png" format from:

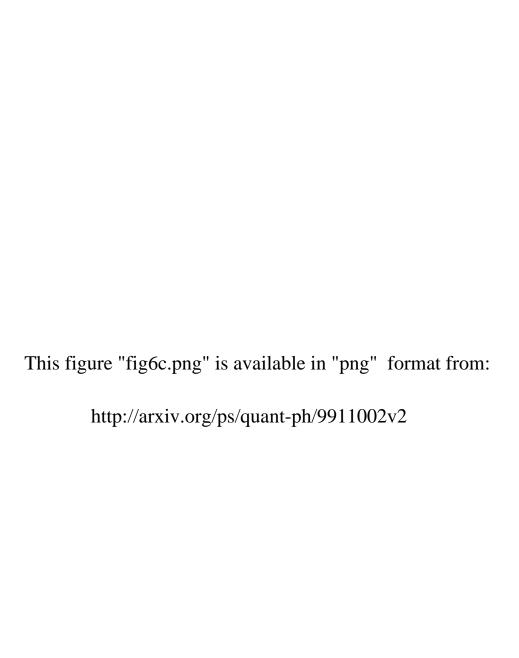
This figure "fig4.png" is available in "png" format from:

This figure "fig5a.png" is available in "png" format from:









This figure "fig7.png" is available in "png" format from: